Journal of Operation and Automation in Power Engineering

vol. 12, no. 4, Dec. 2024, Pages: 337-351

http://joape.uma.ac.ir

Mono ANN Module Protection Scheme and Multi ANN Modules for Fault Location Estimation for a Six-Phase Transmission Line Using Discrete Wavelet Transform

G. Vikram Raju, N. Venkata Srikanth,*

Department of Electrical Engineering, National Institute of Technology, Warangal, India

Abstract— *The enhanced power transfer capability is possible with the six-phase transmission system but it did not gain popularity due to the lack of a proper protection scheme to secure the line from 120 types of different possible short circuit faults. This work presents a protection scheme with discrete wavelet transform (db4 mother wavelet) and an artificial neural network (ANN). The Levenberg-Marquardt algorithm is used for training the ANNs. This protection scheme requires only the pre-processed current information of the sending end bus. For fault detection and classification of all 120 fault types, a single ANN module is implemented with six inputs and six outputs. For fault location estimation in each phase, 11 ANN modules with six outputs are implemented, one for each of the 11 types of combination of faults. The MATLAB/ SIMULINK simulation results of the proposed protection technique implemented on the six-phase Allegheny power transmission system show that it is effective and efficient in detecting and classifying all the faults with varying fault parameters with an accuracy of 99.76%. It is found that the performance of the fault location estimation modules is better with the training data and moderate with the testing data.*

Keywords—Artificial neural network, Discrete wavelet transform, Fault detection/ classification, Fault location estimation, Six-phase transmission.

NOMENCLATURE

Abbreviations

Φ	Fault inception angle
L_a	Actual fault location
mse	Mean squared error
std	Standard deviation
T_f	Time of fault/ fault inception time
E_{fl}	Estimated fault location
R_f	Fault resistance
ANN	Artificial neural network
ANN_FDC	Artificial neural network_Fault detection and classification
ANN_FLE	Artificial neural network_Fault location estimation
DFT	Discrete Fourier transform
DWT	Discrete wavelet transform
EHV	Extra high voltage
FDC	Fault detection and classification
FI	Fault index
FIA	Fault inception angle
FIT	Fault inception time
FLE	Fault location estimation
HPF	High-pass filter
HVDC	High voltage direct current
LMA	Levenberg-Marquardt algorithm
LPF	Low-pass filter
NF	No-fault

Received: 18 Oct. 2022
Revised: 16 Jan. 2023
Accepted: 22 Apr. 2023
*Corresponding author:
E-mail: gottevr@student.nitw.ac.in (G. Vikram Raju)
DOI: 10.22098/joape.2023.11690.1874
Research Paper

1. INTRODUCTION

The nations across the world aimed at reducing the carbon emissions by encouraging the renewable energy sources to generate the clean energy. Despite the global economic crisis in 2020, there is a record rise in the global renewable energy generation capacity i.e., 260 GW during COVID 2019 pandemic. Solar (127 GW) and wind (111 GW) dominated this capacity expansion by 91% [1]. The resulting intermittent generation and centralized demand require increased transmission capacities. In many countries, obtaining a new right of way to build an overhead line is very difficult. Building a new transmission line corridors is quite expensive and time-consuming process. Also encounters the land availability problem and an opposition from the environmentalists for the ecological reasons. In the pursuit of meeting the increasing power demands, the generation or power transfer capabilities of the transmission network have to be increased. The environmental, economic, and land availability concerns for building the new transmission infrastructure to have enhanced power transfer capabilities, led the power system engineers to search for alternate methods. The extra-high voltage (EHV) transmission lines can serve the purpose but the EHV lines produce strong electric fields at the ground surface, possible biological effects, visual pollution, and audible noise. HVDC transmission is another alternative but the demerit is that it requires huge capital for installation and operation. In 1972, H. C. Barnes and L.D. Barthold has proposed the high phase order transmission systems for maximizing the power density by employing the existing transmission corridors efficiently. The high phase order transmission is a viable solution. The six-phase transmission with the existing three-phase double circuit transmission line without major alterations paved the way with 73 % more power transfer capability. The other benefits of six-phase transmission over three-phase transmission are i) reduced

Table 1. Types and no. of short circuit faults on six-phase transmission line.

Fault type	1-LG	2-L	2-LG	3-L	3-LG	4-L	4-LG	5-L	5-LG	6-L	6-LG
No. of faults	6	15	15	20	20	15	15	6	6	1	1
Total						120					

phase to phase voltages, ii) current imbalances are minimum – so single-pole switching is possible, iii) reduced radio and audible noise and corona losses are minimum, iv) high compatibility and stability, v) reduced conductor surface gradients, and vi) improved thermal loading capability, surge impedance loading, voltage regulation and better efficiency of lines [2–5]. Now, the countries viz. China and United Kingdom have again started research investigations on upgrading the transmission lines for future needs [6, 7]. The acceptance of the six-phase transmission is vaguely encouraged due to the lack of proper protection schemes to tackle the 120 different types of short circuit faults. Table 1 gives the types of faults on the six-phase system and no. of faults. Fig. 1 shows the flowchart of segregation 120 types of short circuit faults that are possible on six-phase transmission line.

The existing protection schemes available for single/double circuit three-phase transmission systems are not apt for the six-phase transmission system. The number of fault combinations for a three-phase single-circuit and double-circuit transmission line is 11 and 22, but there are 120 types of fault combinations for a six-phase transmission line. The range of fault currents is more and also the complexity of protection scheme increases. The protection schemes developed for the conventional three-phase transmission system either with distance relays or other artificial intelligence-based techniques [8–10] can only utilize the voltage and current information of three phases to detect/classify the fault. But, when these protection schemes are applied to the six-phase line, the relay may or may not operate for all the 120 fault combinations. It is reported that a total of twenty-one conventional distance relays (six for the phase-ground fault detection and fifteen for phase-phase fault detection) are required for the complete protection of six-phase line [11]. Only a few works were reported for the protection of six-phase transmission lines. The fault analysis of the six-phase system with sequence components and phase coordinate method is presented in [2, 4] and fault detection based on negative sequence currents is proposed in [12]. A fault detection and classification technique with discrete Fourier transform (DFT) based ANN is proposed in [5, 13] for only six-phases to ground faults and single-phase to ground faults respectively. A fault classification scheme for phase to phase faults (2 – L faults) is implemented using voltage and current signals in [14] with DWT (Haar wavelet) based ANN approach. The protection for one conductor's open faults in a six-phase transmission system is proposed using ANN in [15]. A complete protection scheme with 22 modular DFT based ANNs (11 – ANNs for FDC and 11 – ANNs for fault location estimation) is presented in [16] which uses voltage and current signals for the protection task. Fault zone identification and fault location estimation with modular ANNs using DWT (db3 wavelet) pre-processed voltage and current signals are proposed [17]. In [18], a hybrid protection scheme is implemented using the harmonic information of voltage signals for FDC with 11 decision tree modules and 11 TLBO tuned ANN modules for fault location estimation. The fuzzy logic-based FDC schemes are presented in [19, 20] using DFT with voltage and current signals. The ANN-based protection schemes reported above have either considered only one type of fault viz. single phase to ground, six-phase to ground, and phase to phase faults or modular ANN methods for fault detection and classification. Only a few works have reported the fault location estimation. In the present work, a complete protection scheme (fault detection/classification and fault location estimation) is proposed using only the phase current information of the sending end bus with discrete wavelet transform (DWT) and artificial neural networks. Unlike the earlier works, the proposed scheme implemented only a single module of ANN for fault detection and classification. For fault location estimation, the modular ANN method is implemented where each ANN module gives the fault location estimation in all six phases.

Table 2. Basic system description data

System Voltage	138 kV
No. of phases	6
No. of circuits	1
No. of sub-conductors per phase	1
Total no. of ground wires	2
Earth resistivity	100 Ω-m
Frequency	60 Hz
Base voltage	138 kV
Base power	100 MVA
Line length	68 km

2. Six phase transmission system

The six-phase Allegheny's power transmission system is considered for the present work referring to the line between the buses Springdale and McCalmont [3]. It consists of a 138 kV, 60 Hz single circuit six-phase transmission line of 68 km length fed from the sources at both the ends (sending and receiving ends) of the line. The sending end (source-1) and receiving end (source-2) source impedances are $2.03 + j9.04\Omega$ and $4 + j17.94\Omega$ with short circuit capacities of 1.25 GVA respectively. Two loads (load-1, 80 MW and load-2, 60 MVar) are connected at the receiving end bus B2. Fig. 2 shows the one-line diagram of the considered six-phase power system network along with a block diagram of the proposed protection scheme. The DWT-ANN based relay is installed at the sending end bus, B1.

However, the maximum number of phases of a transmission line apart from six-phase can be nine, twelve or even twenty-four phases i.e., multiples of conventional three-phase system to provide interfacing with the existing three-phase system through transformers. Different tower structures are analysed to have simple and compact spacing of lines with minimum insulation cost. The fact that the adjacent phase to phase voltages is less in high-phase order systems compared to the conventional three-phase system made it possible for the compaction of the lines [21]. For six and twelve phase configurations, the hexagonal placement is preferred. Generally, the phase conductors are placed sequentially on the vertices and/or on the edges of the hexagon. The Fig. 3 (a) and 3 (d) shows an example of the schematic of the phases on the tower of a six-phase and twelve-phase transmission line. However, due to transposition of phases, each position is occupied by every phase in the order of phase sequence.

Tables 2 and 3 depict the basic system description and the line configuration data of the six-phase system considered in the present work. The model used in the work takes into account the distributive nature of the transmission line by considering the uniform distribution of resistance, inductance and capacitance along the line length. The six-phase transmission line model is implemented and simulation studies are carried out using the software MATLAB®/Simulink platform.

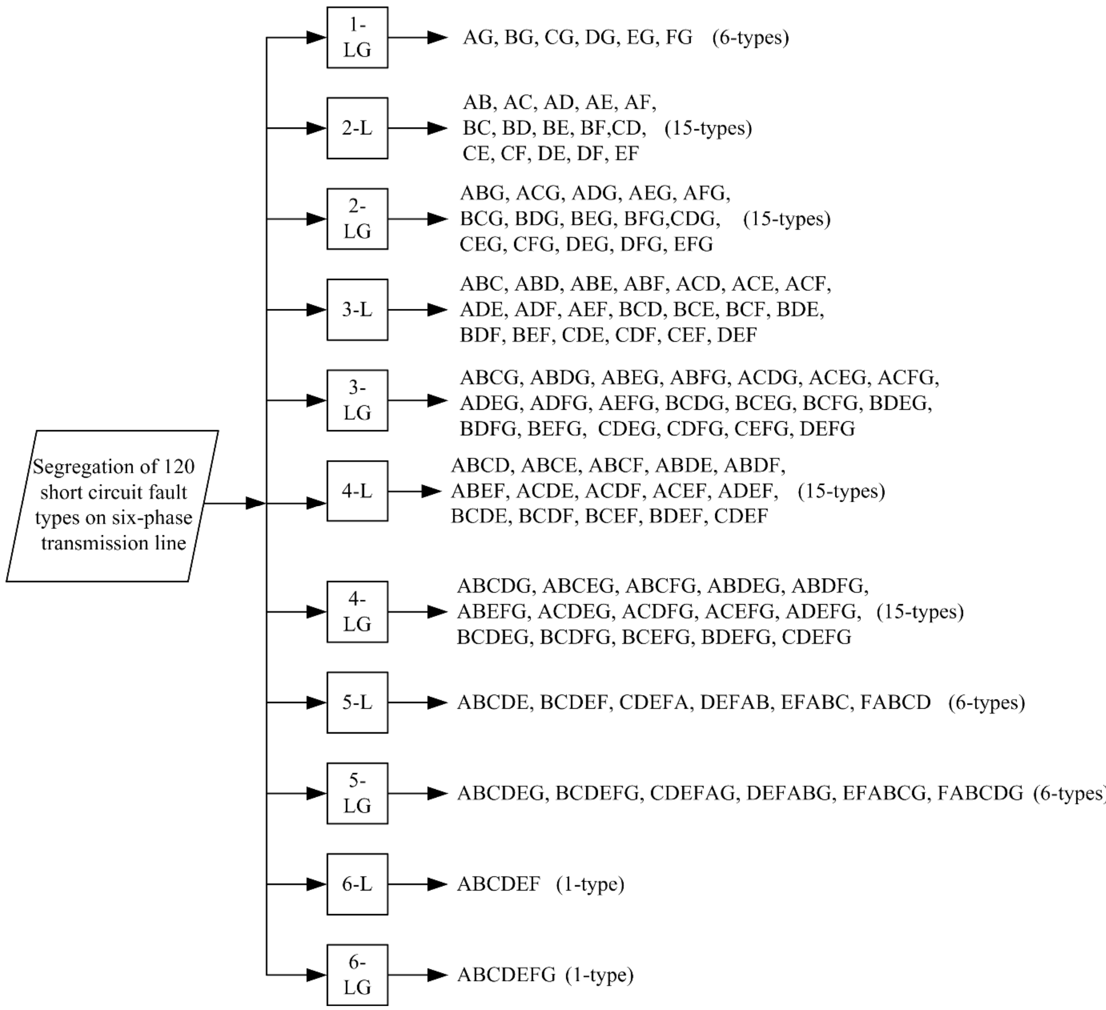

Fig. 1. Flowchart of segregation of 120 types of short circuit faults

Table 3. Line configuration data

Phase no.	Conductor designation	Horizontal spacing X (ft)	Height at tower Y (ft)	Mid-span clearance (ft)
1	*a*	-11	68	56
2	*b*	-14	55	43
3	*c*	-11	42	30
4	*d*	11	42	30
5	*e*	14	55	43
6	*f*	11	68	56
0	*GR1*	-6	77.5	67.1
0	*GR2*	6	77.5	67.1

3. Proposed protection scheme using the DWT and ANN for six-phase transmission system

From the protection point of view, any short circuit fault has to be detected and isolated as early as possible to mitigate the effect of the fault on the system and to estimate the fault location accurately to send the repairmen's crew. In the present work, a protection scheme is proposed for the six-phase transmission system shown in Fig. 2 using the discrete wavelet transform and artificial neural network. With the proposed protection scheme, two protection tasks are accomplished. The first task is to identify and classify the fault and the second task is to estimate the fault location. There are two stages in the proposed protection scheme, i) feature extraction process and ii) actual protection scheme implemented using the ANNs.

To implement any digital protection scheme, a proper feature of the system (either voltage/ current) has to be used to accomplish the protection task. The recorded time-domain raw data of instantaneous voltage/ current signals available at the relaying point may not be used as such, so to extract the useful features from the raw data, a transform has to be used to convert the signal to frequency domain or time-frequency domain. Discrete wavelet transform (DWT) is one of the most widely used signal processing techniques in engineering domains which analyses the signal both in time and frequency domains. This transform has gained a lot of popularity in power system protection because it efficiently analyses the non-stationary signals and localizes the signal in time and frequency domains. In DWT, the signal is decomposed into a number of levels where each level corresponds to a particular frequency band. This transform provides the degree of similarity between the signal to be analysed and the analysing signal in terms of detail coefficients (higher frequency components) and approximate coefficients (lower frequency components). The proper selection of the mother wavelet plays an important role

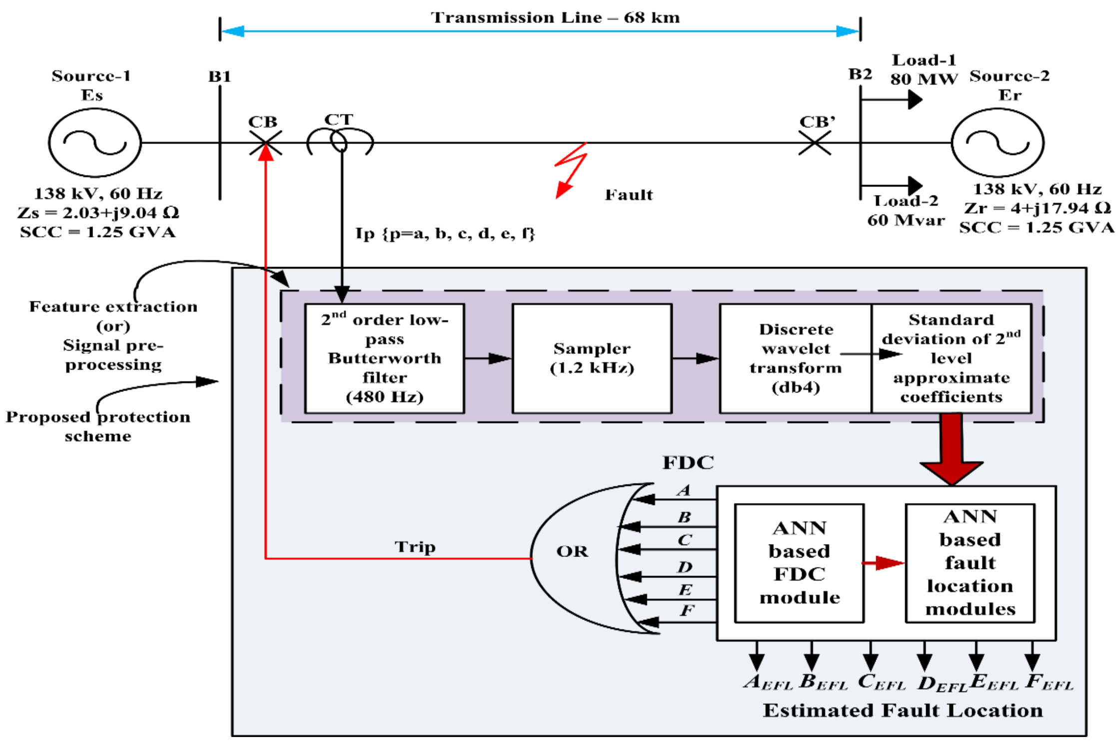

Fig. 2. One-line diagram of the considered six-phase transmission system along with a block diagram of the proposed protection scheme.

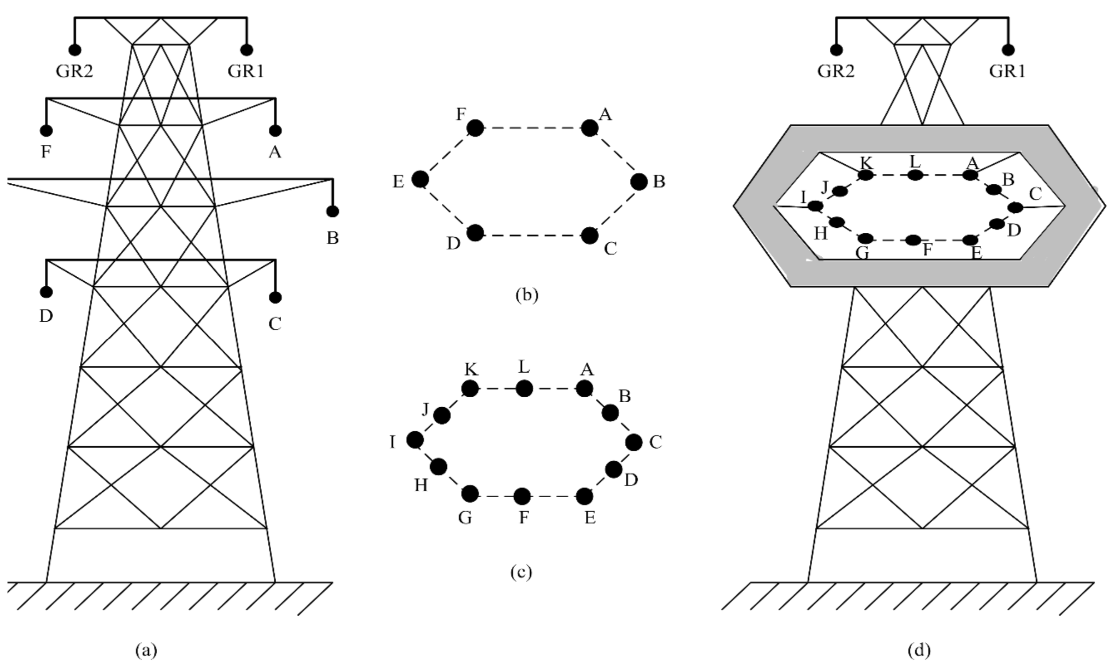

Fig. 3. Schematic of tower structures (a) and (b) six-phase line, (c) and (d) twelve-phase line

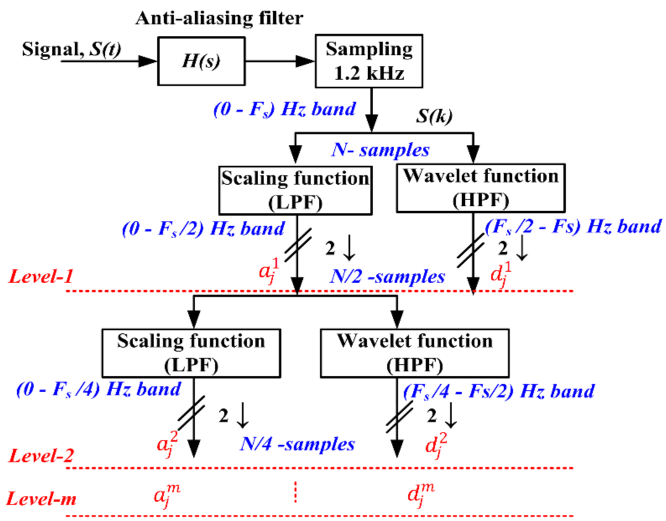

Fig. 4. Signal pre-processing and DWT decomposition

in analysing the signal [17, 22–24]. A schematic diagram of the signal decomposition by DWT is shown in Fig. 4. In the present work, the instantaneous current signals in each phase of the sending end bus (B1) are employed for the protection task. The instantaneous current signals of bus B1 are pre-processed with the second-order low-pass Butterworth filter (anti-aliasing filter) with a cut-off frequency of 480 Hz to eliminate the higher-order harmonics in the signal. Butterworth filters are used because they provide maximum flat characteristics in the passband region. Eq. (1) gives the general expression for the n^{th} order low-pass Butterworth filter. These filtered signals are sampled at a 1.2 kHz sampling frequency (20 samples per one cycle data of 60 Hz frequency) according to the Nyquist sampling criteria. The expression for the second-order low-pass Butterworth filter with a cut-off frequency of 480 Hz and Nyquist sampling frequency of 1.2 kHz is given in Eq. (2). The DWT is implemented on the sampled current signals with the Daubechies wavelet db4 is used as the mother wavelet. The standard deviation (*std*) of the second level approximate coefficients of current signals in each phase is used as the features for the protection scheme. The basic expression for the DWT of a signal *S(t)* is given in Eq. (3), where *S(k)* is sampled signal, b_0^m is the scaling parameter, kb_0^m is the translation parameter, and Ψ is the mother wavelet [25].

$$H\left(s\right)=\frac{y\left(1\right)s^{n}+y\left(2\right)s^{n-1}+\cdots+y(n+1)}{x\left(1\right)s^{n}+x\left(2\right)s^{n-1}+\cdots+x(n+1)} \quad (1)$$

$$H\left(s\right)=\frac{0.6389s^{2}+1.2779s+0.6389}{s^{2}+1.143s+0.4128} \quad (2)$$

$$DWT\left(S,m,n\right)=\frac{1}{\sqrt{b_0^m}}\sum_{k}S(k)\Psi^{*}\left(\frac{n-kb_0^m}{b_0^m}\right) \quad (3)$$

If d_j^m and a_j^m represent the detail and approximate coefficients of m^{th} level of decomposition, then the standard deviation of approximate coefficients is given by the Eq. (4).

$$Standard\ deviation\left(std\right)=\sqrt{\frac{1}{N-1}\sum_{j=1}^{N}\left(a_j^m-\frac{1}{N}\sum_{j=1}^{N}a_j^m\right)^{2}} \quad (4)$$

Where N is the no. of coefficients. The process of calculating the standard deviation of second-level approximate coefficients of current signals is carried out consecutively for each cycle window of 20 instantaneous current samples, viz window-1 of 1-20 samples, window-2 of 2-21 samples, and so on. Therefore, the required features obtained after the feature extraction process are std_a, std_b, std_c, std_d, std_e, and std_f for each of the six phases.

Table 4. Fault parameter variations considered in the training and testing data samples

S. N0.	Fault Parameter	Variations considered	
		In the training data	In the testing data
1.	Fault resistance (Ω)	0.01 Ω, 50 Ω, and 100 Ω	30 Ω and 70 Ω
2.	Fault inception angle (°)	0° and 90°	0° and 45°
3.	Fault location (km)	1 km, 4 km, 8 km, . . . , 64 km, and 67 km (18-locations)	1 km, 6 km, 12 km, . . . , 60 km, and 66 km (12 - locations)
4.	No. of fault types	120	120
5.	Total no. of fault cases considered	$3*2*18*120=12960$; 1-no fault case	$2*2*12*120=5760$; 1-no fault case

ANNs have gained a lot of importance in the engineering domains, especially for the protection of three-phase single-circuit and double circuit transmission lines for their ability of the self-adaptability to the varying operating conditions, non-linear function approximation, pattern recognition, and learning capabilities. The main advantage of ANN is the high-speed online computation. The feedforward neural networks with the Levenberg-Marquardt training algorithm are implemented using MATLAB for fault detection/ classification and fault location estimation. The flow chart for the Levenberg-Marquardt algorithm (LMA) is given the Fig. 5. The Levenberg-Marquardt algorithm is the fastest algorithm. It takes lesser execution for training the ANN [26].This optimization algorithm is an iterative method used to solve the non-linear least square problems. It is a combination of the Gauss-Newton method and gradient descent method [27, 28]. For training the ANN, LMA is used to learn the weights and biases of the neural network. The advantage of the Levenberg-Marquardt algorithm, it attains second-order training speed without the requirement to calculate the Hessian matrix.

There is no hard and proven rule to achieve the optimal architecture (no. of hidden layers and no. of neurons) of the artificial neural network (ANN). A series of pilot runs based on hit-and-trail basis method is the general process for selecting the architecture of ANN. The features that should be taken care while training the ANN are architecture, neural network parameters (weights and biases), type of activation function, and training/learning algorithm.

Unlike the modular ANNs reported earlier for fault detection and classification of 120 types of faults, the present work proposed a single ANN_FDC module with the standard deviation of second-level approximate coefficients of six-phase currents of sending end bus as inputs and six outputs (*A, B, C, D, E,* and *F*) one for each phase for faulty phase detection and classification of faults. The most important tasks in training the ANN are the generation of training samples, preparation of input training and target data sets, selecting the optimum no. of hidden layers, and choosing the activation functions for the proper pattern recognition. The training and the testing data samples are generated by simulating the different types of faults with varying fault locations, fault inception angles, and fault resistances on the six-phase transmission system shown in Fig. 2 on the MATLAB®/ Simulink platform.

Table 4 presents the different fault parameter variations considered for generating the training and testing data samples. Ten post-fault samples data of the standard deviation of second-level approximate coefficients of sending end bus phase currents are collected for each of the simulated faults and hence the training data set is created. Table 5 presents the number of samples collected for each type of fault for the training and testing data sets. For the fault detection in each phase and classification purpose, the ANN_FDC module outputs are labelled as *'+1'* and

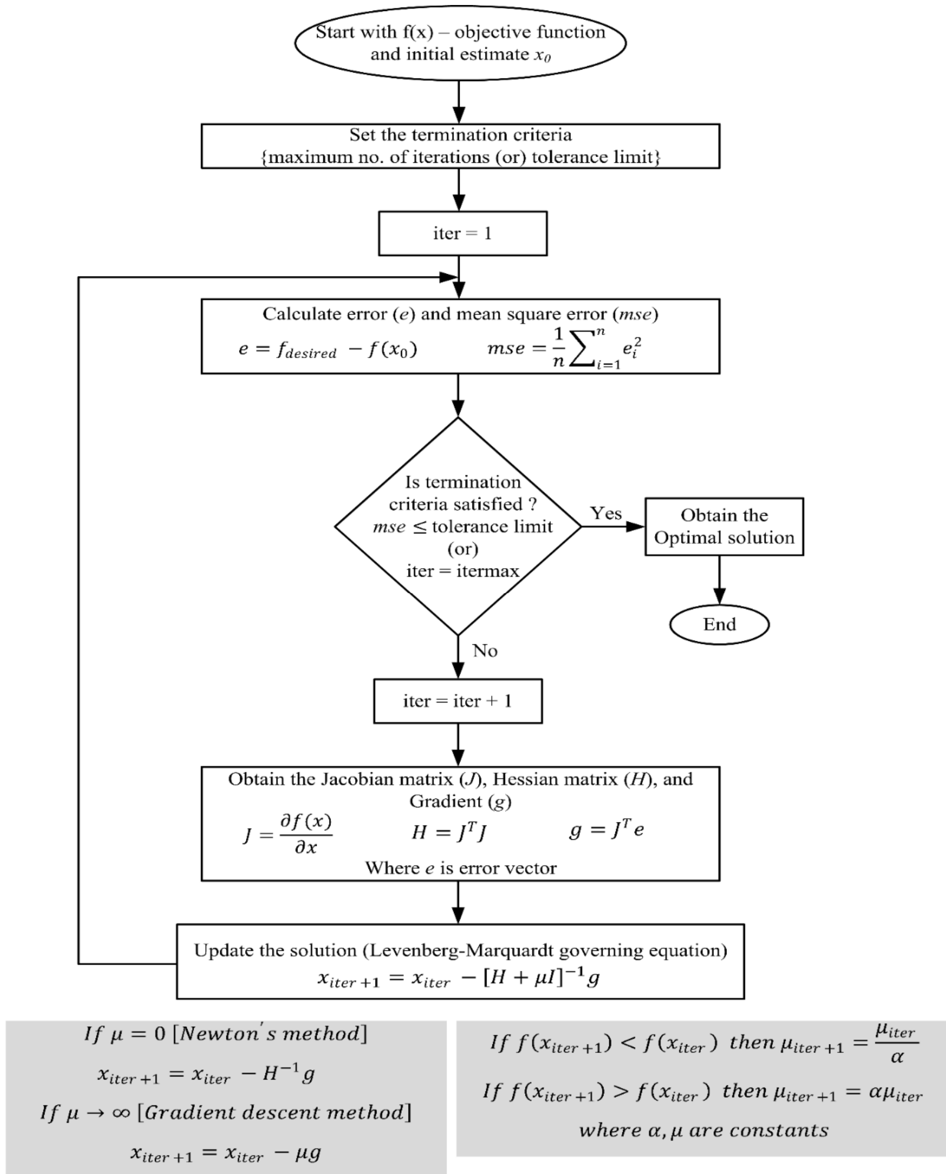

Fig. 5. Flow chart of Levenberg-Marquardt algorithm

'-1'. The output *'+1'* is used to indicate the fault condition and *'-1'* is used to indicate the healthy/ no-fault (NF) condition in the particular phase.

In order to select the optimal architecture of the ANN for fault detection and classification, a no. of pilot runs was carried out with the generated training data with different no. of hidden layers and neurons, and with different activation functions on a trial-and-error basis method. The optimal architecture of ANN_FDC, type of activation functions, training input and output data sizes, and mean square error achieved during training are presented in Table 6 for the fault detection and classification module. Fig. 6 presents the architecture 6-18-18-6 of the ANN_FDC module with 6 – input neurons, 18 – neurons each in the two hidden layers, and 6 – output layer neurons with tansig activation function in all the layers. Fig. 7 presents the mean squared error (*mse*) achieved during the training process of the ANN_FDC module.

For identifying the involvement of ground in the grounded faults, in 1998, M. Akke and J. T. Thorp [29] proposed a current index that separates the faults with zero-sequence currents from the faults without zero sequence currents for a three-phase system. The fault index expression that is used to identify the grounded faults is given in Eq. (5) for an *'n'* phase system.

$$Current\ index\ or\ Fault\ index\ (FI) = \frac{\sum |I_p|}{median\,(|I_1|, |I_2|, \ldots, |I_p|)} \quad \text{where } p = 1,\ 2,\ \ldots,\ n\ phases \tag{5}$$

$$If\ FI > 0.05,\ then\ ground\ is\ present.$$

$$If\ FI \leq 0.05,\ then\ ground\ is\ absent.$$

In the present study, the above current index has been extended up to the six-phase system (*n = 6 phases i.e., p = a, b, c, d, e, and f phases*) and instead of fault index, standard deviation of fault index is used to detect the ground involvement in the fault given

Table 5. Number of training and testing data samples collected for each type of fault

S. No.	Fault type	Training		Testing	
		No. of cases	No. of samples	No. of cases	No. of samples
1.	1-LG and No fault	(6*3*2*18)+1 = 648+1=649	649*10 = 6490	(6*2*2*12)+1 = 288+1=289	289*20 = 5780
2.	2-LG and 2-L	(15*3*2*18)+(15*3*2*18) = 1620+1620 = 3240	3240*10 = 32400	(15*2*2*12)+(15*2*2*12) = 720+720 = 1440	1440*20 = 28800
3.	3-LG and 3-L	(20*3*2*18)+(20*3*2*18) = 2160+2160 = 4320	4320*10 = 43200	(20*2*2*12)+(20*2*2*12) = 960+960 = 1920	1920*20 = 38400
4.	4-LG and 4-L	(15*3*2*18)+(15*3*2*18) = 1620+1620 = 3240	3240*10 = 32400	(15*2*2*12)+(15*2*2*12) = 720+720 = 1440	1440*20 = 28800
5.	5-LG and 5-L	(6*3*2*18)+(6*3*2*18) = 648+648 = 1296	1296*10 = 12960	(6*2*2*12)+(6*2*2*12) = 288+288 = 576	576*20 = 11520
6.	6-LG and 6-L	(1*3*2*18)+(1*3*2*18) = 108+108 = 216	216*10 = 2160	(1*2*2*12)+(1*2*2*12) = 48+48 = 96	96*20 = 1920
7.	Total	12961	129610	5761	115220

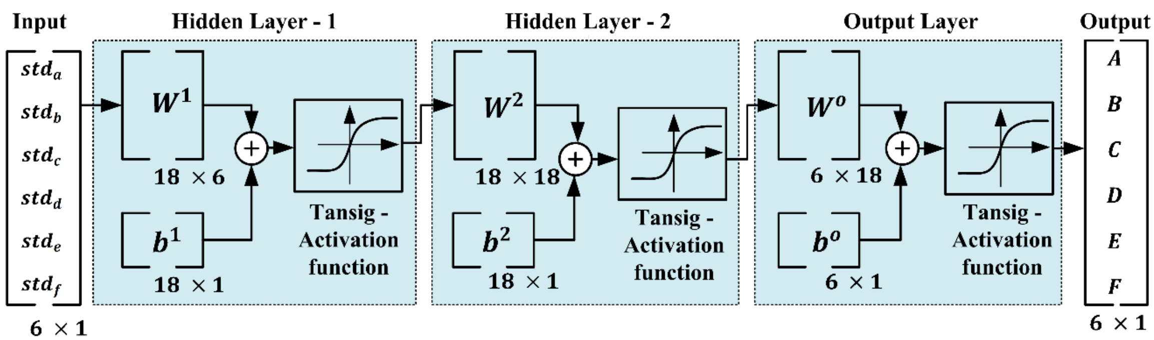

Fig. 6. Architecture of ANN_FDC module.

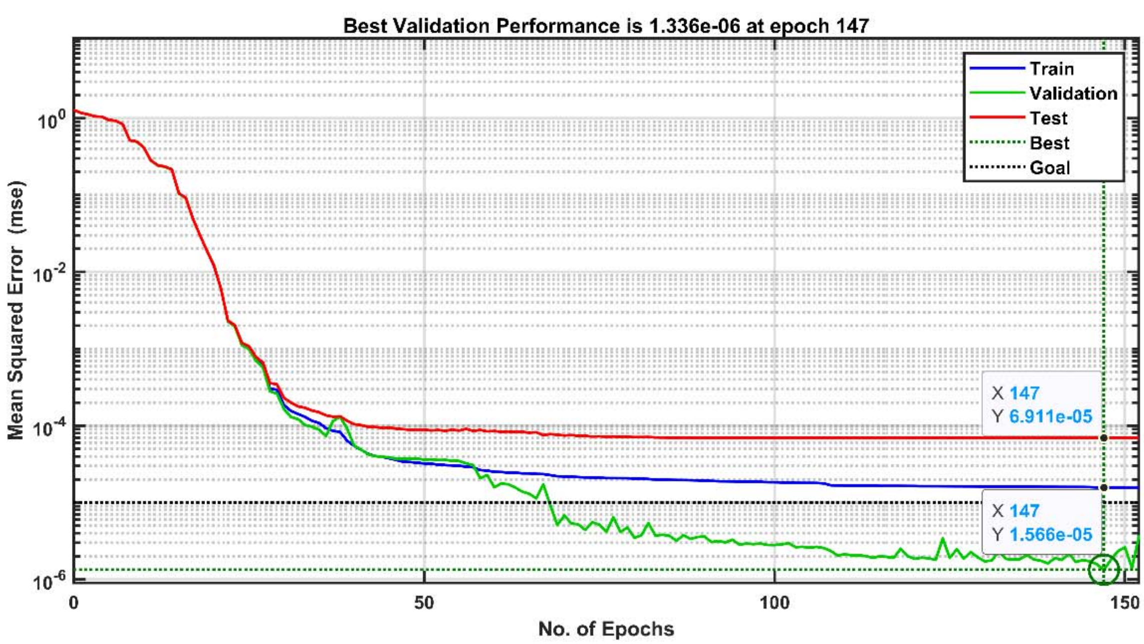

Fig. 7. Mean squared error achieved during the training of the ANN_FDC module.

in Eq. (6) and Eq. (7).

$$Standard\ deviation\ \ (std_{FI}) = \sqrt{\frac{1}{M-1}\sum_{j=1}^{M}\left(FI_j - \frac{1}{M}\sum_{j=1}^{M}FI_j\right)^2} \quad (6)$$

$$where\ M = no.\ of\ current\ samples\ per\ 60\ Hz\ cycle.$$

$$Ground\ \ (G) = \begin{cases} +1,\ if\ std_{FI} > 0.05,\ then\ ground\ is\ present \\ -1,\ if\ std_{FI} \leq 0.05,\ then\ ground\ is\ absent \end{cases} \quad (7)$$

Where std_{FI} is the standard deviation of fault index, I_a, I_b, I_c, I_d, I_e, and I_f are the six-phase instantaneous currents of the bus B1. The involvement of ground is detected with *'+1'* when the std_{FI} is greater than the threshold and *'-1'* is used to identify that no involvement of ground in the fault. In the present work, there are eleven ANN modules for fault location estimation (FLE), one for each type of fault. In all the ANN fault location estimation modules, there are six inputs and six outputs one for each phase. The input training data set to the ANN_FLE modules is the standard deviation of second-level approximate coefficients of the currents of bus B1 with the fault parameters shown in Table 4. For training the ANN_FLE modules, the target data set is created with the actual fault locations for the faulty phases and healthy phases are labelled with 140 km. A series of trails are run with the training data to select the best ANN_FLE modules. The architecture, type of activation function, input and output data size, and mean square error (*mse*) achieved during training of the best ANN_FLE modules are shown in Table 6. The tansig activation function is used for the hidden layers and the purelin activation function is used for the output layers of ANN fault location estimation modules.

The flow chart of the proposed protection scheme is shown in Fig. 8. In the proposed protection scheme, the single-end pre-processed current data is fed to all 12 ANN modules simultaneously. The ANN_FDC module output and FI output information are used for the fault detection/ classification purpose and based on fault type information the particular fault type of the ANN_FLE module is selected to have the estimated fault location in each phase. The '*OR*' operation on the ANN_FDC module outputs is used to generate the trip signal to the circuit breakers.

4. Results and Discussion

The performance of the proposed protection scheme has been evaluated by conducting a series of simulations by varying the fault parameters viz. fault resistance (R_f) (0–100) Ω, fault inception angle (*Φ*) (0°– 360°), and fault location (L_f) (1–68) km. Further, to validate the proposed protection scheme, testing data that is different from the training data is generated using the fault parameters shown in Table 4 and the no. of fault cases (5761) and samples considered (115220) is shown in Table 5. The accuracy and the dependability of the proposed protection scheme for fault detection and classification are assessed w.r.t training and testing data using the confusion matrices. The accuracy and dependability are evaluated as [18]

$$Accuracy = \frac{total\ no.\ of\ fault\ cases\ predicted\ correctly}{total\ no.\ of\ actual\ fault\ cases\ and\ no\ fault\ cases} \times 100 \quad (8)$$

$$Dependability = \frac{total\ no.\ of\ fault\ cases\ predicted\ correctly}{total\ no.\ of\ actual\ fault\ cases} \times 100 \quad (9)$$

The performance of the protection scheme for the fault location estimation for all the fault location modules is evaluated in terms of percentage error in the estimated fault location for all the phases as [17]

$$\%\ Error\ in\ the\ estimated\ fault\ location\ (\%E) = \frac{E_{fl} - L_a}{total\ length\ of\ the\ line} \times 100 \quad (10)$$

Where E_{fl} and L_a are the estimated fault location and actual fault location.

The fault detection/ classification of the proposed protection scheme is effective and efficient even with the variation of fault parameters. A four-phase to ground fault (4-LG, (ABCDG)) is simulated at fault location (L_a) of 10 km from bus B1 with fault resistance (R_f) 30 Ω and fault inception angle (Φ) of 0° (fault inception time (T_f) 0.05 s) and the six-phase instantaneous currents at bus B1 are shown in Fig. 9(a). Fig. 9(b) presents the standard deviation of the second level approximate coefficients of the current signals i.e., pre-processed input features by DWT to ANN modules. Fig. 9(c) presents the standard deviation of the fault index i.e., used for the ground detection. Fig. 9(d) shows the fault detection and classification outputs for the ANN_FDC module where the faulty phases are detected as a fault with the level of output *'+1'* after the inception of fault while the healthy phases are shown with *'-1'* level of output. Hence the ANN_FDC module clearly identifies and classifies the fault as ABCDG fault with maximum and minimum FDC time as 2.5 ms (0.0525 ms - 0.05 ms = 2.5 ms) and 3.33 ms (0.0533 ms – 0.05 ms = 3.33 ms) which is much less than one cycle time (16.67 ms).

The performance of the ANN_FDC module for varying fault resistance is evaluated and the results are tabulated in Table 7. The fault location and the fault inception angle (fault inception time) are kept constant at 34 km and 0° (0.05 s) and the different faults are simulated with different resistances. It can be observed from Table 7 that the proposed ANN_FDC module correctly identifies the faults within 7 ms time (less than one cycle time).

The performance of the ANN_FDC module for varying fault locations is evaluated and the results are tabulated in Table 8. The fault resistance and the fault inception angle (fault inception time) are kept constant at 75 Ω and 0° (0.05 s) and the different faults are simulated at different fault locations. It can be observed from Table 8 that the proposed ANN_FDC module correctly identifies the faults within 9 ms time (less than one cycle time).

The performance of the ANN_FDC module for varying fault inception angles is evaluated and the results are tabulated in Table 9. The fault resistance and the fault location are kept constant at 90 Ω and 50 km, and the different faults are simulated at different fault inception angles. It can be observed from Table 9 that the proposed ANN_FDC module correctly identifies the faults within 8 ms time (less than one cycle time). To obtain the overall assessment of the proposed fault detection and classification of the ANN_FDC module, confusion matrices w.r.t to training and testing data is presented in Table 10 and Table 11. The true and predicted fault types are represented on the left and top of the tables.

The accuracy and the dependability of the proposed protection scheme w.r.t fault detection and classification are given in Table 12. From the table, it can be understood that the proposed method's performance is efficient and accurate in the FDC task.

The performance of the proposed protection scheme ANN_FLE fault location estimation modules detailed in Table 6 is evaluated for the different faults simulated i.e., with varying fault parameters. A single line to ground fault (AG) is simulated at a fault location of 65 km from bus B1 at 0.05 s with a fault resistance of 80 Ω and a double line to ground fault (ABG) is simulated at a fault location of 1 km from bus B1 at 0.05 s with fault resistance of 60 Ω. The response of the ANN_FLE_1-LG module for the AG fault and the ANN_FLE_2-LG module for the ABG fault is shown in Fig. 10 and Fig. 11. It can be observed from Fig. 10 that the proposed ANN_FLE_1-LG module approximately estimates the actual fault location for the faulty phase (A-phase) as 65.3 km while the healthy phases as 140 km. Similarly, the estimated fault location is obtained as 0.8737 km and 0.9271 km as depicted in Fig. 11 for the faulty phases. Some of the test results of the proposed ANN_FLE modules are depicted in Table 13, Table 14, and Table 15 for different faults. It is evident from the test results in Fig. 10, Fig. 11, and Tables 13, 14, and 15 that the proposed method provides approximately near-fault location estimation results.

Table 6. Details of ANN architecture for FDC and fault location estimation

S. No.	ANN for	Architecture	Activation function	Input & output data size	MSE achieved during training
1.	ANN_FDC	6-18-18-6	Tansig	6 × 129610	1.336e-06
2.	ANN_FLE_1-LG	6-25-25-6	Tansig & purelin	6 × 6490	9.97e-07
3.	ANN_FLE_2-L	6-25-25-25-6	Tansig & purelin	6 × 16210	1.70e-05
4.	ANN_FLE_2-LG	6-25-25-25-6	Tansig & purelin	6 × 16210	1.22e-05
5.	ANN_FLE_3-L	6-25-25-25-25-6	Tansig & purelin	6 × 21610	1.59e-04
6.	ANN_FLE_3-LG	6-30-30-30-6	Tansig & purelin	6 × 21610	9.03e-05
7.	ANN_FLE_4-L	6-25-25-25-25-6	Tansig & purelin	6 × 16210	3.68e-05
8.	ANN_FLE_4-LG	6-25-25-25-25-6	Tansig & purelin	6 × 16210	3.22e-05
9.	ANN_FLE_5-L	6-25-25-25-6	Tansig & purelin	6 × 6490	3.84e-06
10.	ANN_FLE_5-LG	6-30-30-30-6	Tansig & purelin	6 × 6490	5.52e-06
11.	ANN_FLE_6-L	6-15-15-6	Tansig & purelin	6 × 1090	9.97e-07
12.	ANN_FLE_6-LG	6-15-15-6	Tansig & purelin	6 × 1090	1.00e-06

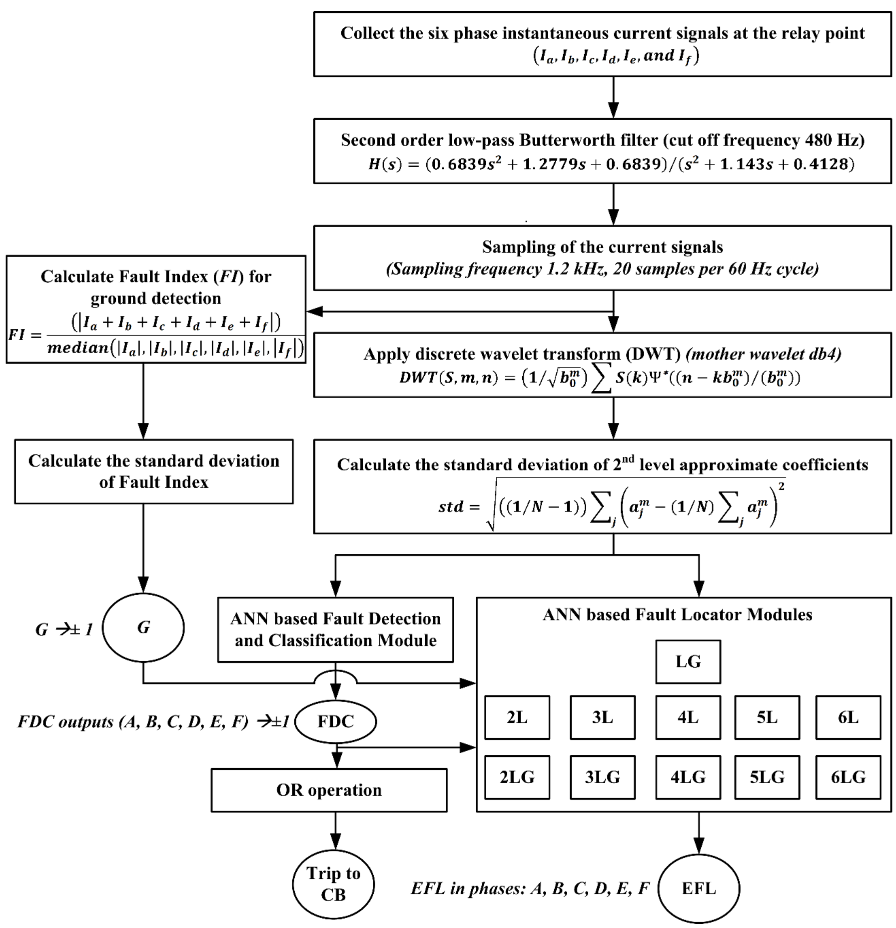

Fig. 8. Flow chart of the proposed protection scheme.

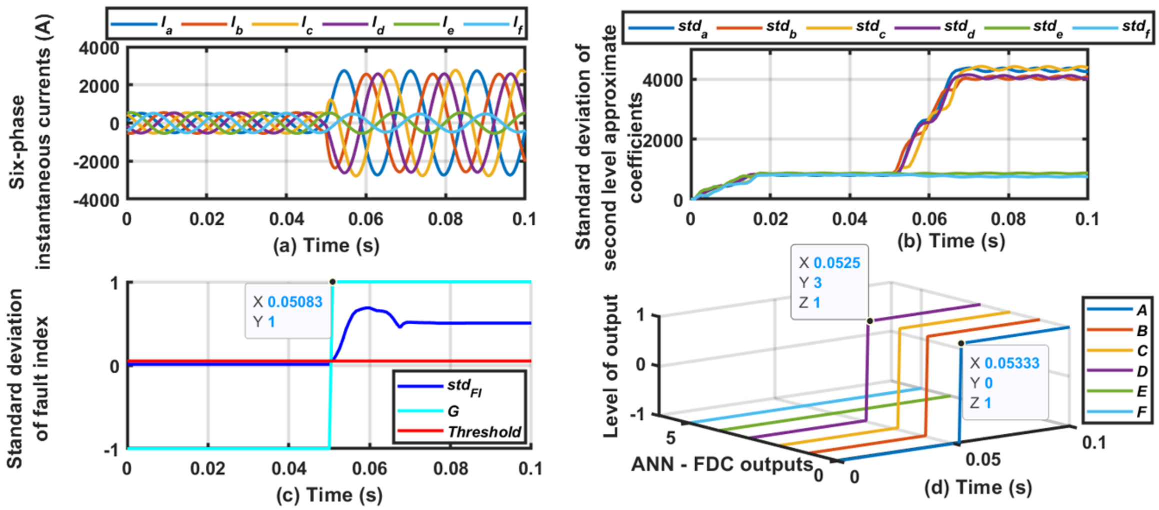

Fig. 9. **(a)** Six phase instantaneous currents, **(b)** Input patterns for the ANN_FDC module, **(c)** Fault index for ground detection, and **(d)** ANN-based Fault detection and classification module outputs.

Table 7. Results of the ANN_FDC module for the varying fault resistance

S. No.	Fault type with varying R_f (Ω) L_f = 34 km, FIA $(\Phi^{\circ}) = 0^{\circ}$ (FIT = 0.05 s)	ANN_FDC module outputs							FDC time (ms)	
		A	*B*	*C*	*D*	*E*	*F*	*G*	Min.	Max.
1.	CG with 70 Ω	-1	-1	1	-1	-1	-1	1	5.83	5.83
2.	BDE with 5 Ω	-1	1	-1	1	1	-1	-1	1.67	5.0
3.	CDFG with 25 Ω	-1	-1	1	1	-1	1	1	2.5	6.67
4.	ACDE with 10 Ω	1	-1	1	1	1	-1	-1	2.5	5.83
5.	ABCDFG with 85 Ω	1	1	1	1	-1	1	1	2.5	5.5
6.	ABCDEF with 30 Ω	1	1	1	1	1	1	-1	2.5	5.83

Table 8. Results of the ANN_FDC module for the varying fault location

S. No.	Fault type with varying L_a (km) R_f = 75 Ω, FIA $(\Phi^{\circ}) = 0^{\circ}$ (FIT = 0.05 s)	ANN_FDC module outputs							FDC time (ms)	
		A	*B*	*C*	*D*	*E*	*F*	*G*	Min.	Max.
1.	AG at 3 km	1	-1	-1	-1	-1	-1	1	3.33	3.33
2.	ACG at 20 km	1	-1	1	-1	-1	-1	1	3.33	7.5
3.	BEFG at 40 km	-1	1	-1	-1	1	1	1	2.5	7.5
4.	BCDE at 55 km	-1	1	1	1	1	-1	-1	3.33	8.3
5.	ABCDE at 65 km	1	1	1	1	1	-1	-1	2.5	5.0
6.	ABCDEF at 67 km	1	1	1	1	1	1	-1	2.5	5.83

Table 9. Results of the ANN_FDC module for the varying fault inception angles

S. No.	Fault type with varying FIA (Φ°), (FIT(s)) L_a = 50 km, R_f=90 Ω	ANN_FDC module outputs							FDC time (ms)	
		A	*B*	*C*	*D*	*E*	*F*	*G*	Min.	Max.
1.	FG at 0° (0.05 s)	-1	-1	-1	-1	-1	1	1	6.67	6.67
2.	DF at 45° (0.05208 s)	-1	-1	-1	1	-1	1	-1	2.92	4.59
3.	ACDG at 60° (0.05278 s)	1	-1	1	1	-1	-1	1	3.05	3.89
4.	BCEF at 120° (0.0556 s)	-1	1	1	-1	1	1	-1	3.57	5.23
5.	ACDEF at 180° (0.0583 s)	1	-1	1	1	1	1	-1	2.53	6.7
6.	ABCDEF at 270° (0.0625 s)	1	1	1	1	1	1	-1	2.5	7.5

Table 10. Confusion matrix w.r.t training data

		Predicted faults												
		1-LG	2-L	2-LG	3-L	3-LG	4-L	4-LG	5-L	5-LG	6-L	6-LG	NF	Total
	1-LG	638	-	10	-	-	-	-	-	-	-	-	-	648
	2-L	-	1620	-	-	-	-	-	-	-	-	-	-	1620
	2-LG	-	13	1606	-	1	-	-	-	-	-	-	-	1620
	3-L	-	-	-	2160	-	-	-	-	-	-	-	-	2160
True faults	3-LG	-	-	-	-	2152	-	8	-	-	-	-	-	2160
	4-L	-	-	-	-	-	1620	-	-	-	-	-	-	1620
	4-LG	-	-	-	-	-	13	1607	-	-	-	-	-	1620
	5-L	-	-	-	-	-	-	-	648	-	-	-	-	648
	5-LG	-	-	-	-	-	-	-	-	648	-	-	-	648
	6-L	-	-	-	-	-	-	-	-	-	108	-	-	108
	6-LG	-	-	-	-	-	-	-	-	-	-	108	-	108
	NF	-	-	-	-	-	-	-	-	-	-	-	1	1

Table 11. Confusion matrix w.r.t testing data

		Predicted faults												
		1-LG	2-L	2-LG	3-L	3-LG	4-L	4-LG	5-L	5-LG	6-L	6-LG	NF	Total
	1-LG	288	-	-	-	-	-	-	-	-	-	-	-	288
	2-L	-	720	-	-	-	-	-	-	-	-	-	-	720
	2-LG	-	7	713	-	-	-	-	-	-	-	-	-	720
	3-L	-	-	-	960	-	-	-	-	-	-	-	-	960
True faults	3-LG	-	-	-	-	960	-	-	-	-	-	-	-	960
	4-L	-	-	-	-	-	720	-	-	-	-	-	-	720
	4-LG	-	-	-	-	-	7	713	-	-	-	-	-	720
	5-L	-	-	-	-	-	-	-	288	-	-	-	-	288
	5-LG	-	-	-	-	-	-	-	-	288	-	-	-	288
	6-L	-	-	-	-	-	-	-	-	-	48	-	-	48
	6-LG	-	-	-	-	-	-	-	-	-	-	48	-	48
	NF	-	-	-	-	-	-	-	-	-	-	-	1	1

Table 12. Performance index of ANN_FDC module for FDC

S. No.	Performance index	w.r.t Training data	w.r.t Testing data
1.	Accuracy	$\frac{12916}{12961} \times 100 = 99.65\%$	$\frac{5747}{5761} \times 100 = 99.76\%$
2.	Dependability	$\frac{12915}{12960} \times 100 = 99.645\%$	$\frac{5746}{5760} \times 100 = 99.76\%$

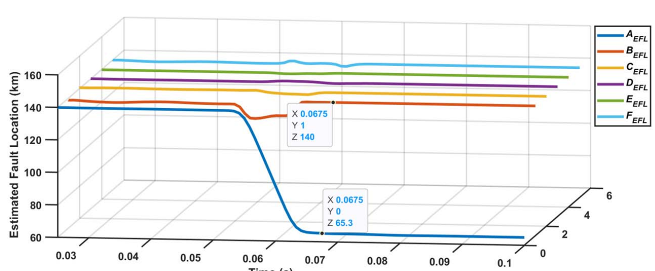

Fig. 10. Estimated fault location by the ANN_FLE_1-LG module for AG fault at 65 km, fault resistance of 80 Ω and fault inception angle of 0° (fault inception time 0.05 s)

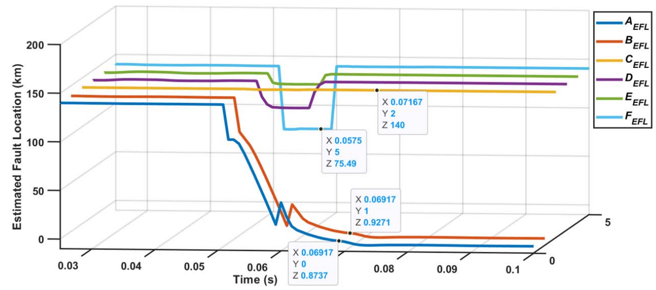

Fig. 11. Estimated fault location by the ANN_FLE_2-LG module for ABG fault at 1 km, fault resistance of 60 Ω and fault inception angle of 0° (fault inception time 0.05 s)

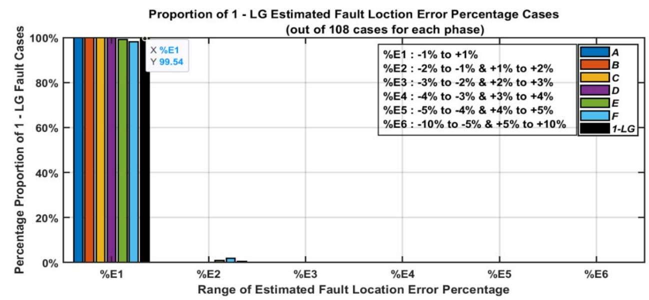

Fig. 12. Proportion of 1-LG estimated fault location error percentage fault cases in different error percentage ranges (w.r.t training data).

Further to analyse the overall performance of the ANN_FLE modules, the training and testing data samples that are given in Table 4 and Table 5 are used to estimate the fault location. The percentage error in the estimated fault location in all the faulty phases is calculated using Eq. (10). Table 16 presents the no. of fault cases for all the phases under each range of percentage error in the estimated fault location for the ANN_FLE_1-LG fault location estimation module w.r.t training data and the same has been depicted in Fig. 12 with the percentage proportion of 1-LG fault cases under each error range. It can be observed that about 99 % of the 1-LG fault cases are within the ±1 % error range.

Similarly, Table 17 presents the no. of fault cases for all the phases under each range of percentage error in the estimated fault location for all the fault location estimation modules w.r.t training data. Fig. 13 with the percentage proportion of fault cases under each error range shown in Table 17. It can be observed that about 81 % of all the fault cases are within the ±1 % error range.

Similarly, Table 18 and Table 19 present the no. of fault cases for each phase for each of the percentage error range for the

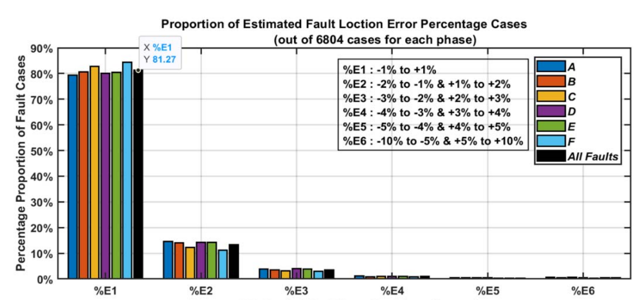

Fig. 13. Proportion of all the estimated fault location error percentage fault cases in different error percentage ranges (w.r.t training data).

Table 13. Estimated fault location by the ANN_FLE modules

Estimated fault location for different faults with R_f = 0.01 Ω, FIA (Φ °) = 0°, and L_a = 5 km Estimated fault location (E_{fl}) in each phase (*km*)								
S. No.	**Fault Type**	A_{EFL}	B_{EFL}	C_{EFL}	D_{EFL}	E_{EFL}	F_{EFL}	**Max. % E**
1.	AG	5.043	140	140	140	140	140	0.063 %
2.	ABG	5.235	5.259	140	140	140	140	0.38 %
3.	ABCG	5.37	5.588	5.437	140	140	140	0.865 %
4.	ABCDG	5.452	5.349	5.463	5.525	140	140	0.772 %
5.	ABCDEG	4.788	4.822	4.831	4.802	4.831	140	-0.311 %
6.	ABCDEFG	4.927	4.927	4.927	4.927	4.927	4.927	-0.107 %
7.	ABCDEF	4.977	4.979	4.977	4.977	4.977	4.98	-0.034 %
8.	ABCDE	5.052	5.053	5.05	5.053	5.032	140	0.078 %
9.	ABCD	5.014	5.215	4.962	5.004	140	140	0.316 %
10.	ABC	5.593	6.035	5.431	139.6	140.2	139.3	1.522 %
11.	AB	4.719	4.932	139.8	140.4	140.1	140.2	-0.413 %

Table 14. Estimated fault location by the ANN_FLE modules

Estimated fault location for different faults with R_f = 90 Ω, FIA (Φ °) = 270°, and L_a = 66 km Estimated fault location (E_{fl}) in each phase (*km*)								
S. No.	**Fault Type**	A_{EFL}	B_{EFL}	C_{EFL}	D_{EFL}	E_{EFL}	F_{EFL}	**Max. % E**
1.	AG	66.1	140	140	139.9	140	140	0.147 %
2.	ABG	66.12	66.26	139.8	140	140	140	0.382 %
3.	ABCG	63.23	63.43	65.25	140.6	140.5	140.2	-4.074 %
4.	ABCDG	66.01	66.21	66.18	66.29	139.9	140	0.426 %
5.	ABCDEG	66.5	66.75	66.72	67.08	140	139.7	2.647 %
6.	ABCDEFG	66.22	66.22	66.22	66.22	66.22	66.22	0.324 %
7.	ABCDEF	66.18	66.18	66.63	66.18	66.18	66.18	0.926 %
8.	ABCDE	66.04	66.17	66.16	66.14	65.3	140	-1.029 %
9.	ABCD	66.32	66.14	66.32	66.38	141.6	138.4	0.559 %
10.	ABC	65.03	67.19	67.28	140.7	140.7	139.4	1.882 %
11.	AB	65.84	65.6	140.9	141.2	140.1	139.5	-0.588 %

Table 15. Estimated fault location by the ANN_FLE modules

		Estimated fault location (E_{fl}) in each phase (*km*)						
S. No.	**Fault Type with R_f (Ω), FIA (Φ °), and L_a(km)**	A_{EFL}	B_{EFL}	C_{EFL}	D_{EFL}	E_{EFL}	F_{EFL}	**Max. % E**
1.	AG with 40 Ω, 0°, and 15 km	14.9	140	140	140	140	140	-0.147 %
2.	ABG with 75 Ω, 30°, and 35 km	35.64	35.83	140	140	140	139.5	1.221 %
3.	ABC with 5 Ω, 60°, and 50 km	49.83	48.95	49.87	140.3	141.1	140.3	-1.544 %
4.	ABCDG with 60 Ω, 90°, and 30 km	29.59	29.55	29.59	29.59	140.1	139.9	-0.662 %
5.	ABCDE with 15 Ω, 120°, and 45 km	43.25	43.24	43.25	43.24	43.24	140	-2.588 %
6.	ABCDEF with 20 Ω, 150°, and 55 km	53.82	53.82	53.82	53.82	53.82	53.82	-1.735 %

Table 16. No. of 1-LG fault cases under each range of percentage error in the estimated fault location (w.r.t training data)

Fault Location Module	Phase	No. of fault cases % E1: -1% to +1%	% E2: -2% to -1% and +1% to +2%	% E3: -3% to -2% and +2% to +3%	% E4: -4% to -3% and +3% to +4%	% E5: -5% to -4% and % +4% to +5%	% E6: -10% to -5% and +5% to +10%
ANN_FLE _1-LG module (108 fault cases for each phase)	A	108	0	0	0	0	0
	B	108	0	0	0	0	0
	C	108	0	0	0	0	0
	D	108	0	0	0	0	0
	E	107	1	0	0	0	0
	F	106	2	0	0	0	0
6 × 108 = 648	1-LG	645	3	0	0	0	0

Table 17. No. of fault cases under each range of percentage error in the estimated fault location (w.r.t training data)

Fault Location Module	Phase	No. of fault cases % E1: -1% to +1%	% E2: -2% to -1% and +1% to +2%	% E3: -3% to -2% and +2% to +3%	% E4: -4% to -3% and +3% to +4%	% E5: -5% to -4% and % +4% to +5%	% E6: -10% to -5% and +5% to +10%
All fault location estimation modules. (6804 fault cases per phase)	A	5403	989	260	79	26	47
	B	5488	954	237	60	29	36
	C	5634	832	210	64	25	39
	D	5443	964	272	73	26	26
	E	5471	968	257	68	21	19
	F	5740	765	198	55	14	32
6 × 6804 = 40824	All faults	33179	5472	1434	399	141	199

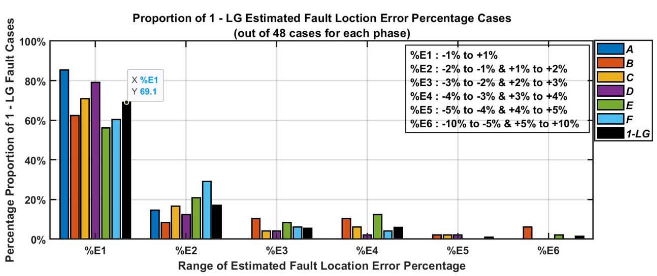

Fig. 14. Proportion of 1-LG estimated fault location error percentage fault cases in different error percentage ranges (w.r.t testing data).

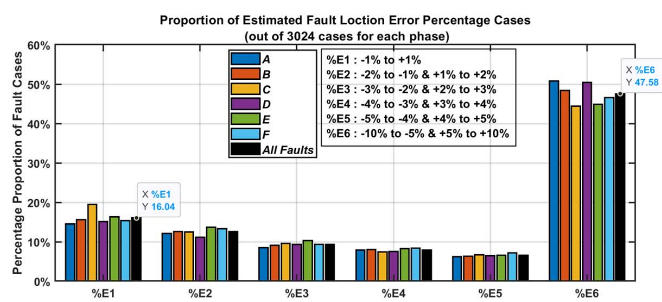

Fig. 15. Proportion of all the estimated fault location error percentage fault cases in different error percentage ranges (w.r.t testing data).

ANN_FLE_1-LG module and all the fault location estimation modules w.r.t testing data. Fig. 14 and Fig. 15 present the proportion percentage of faults cases for each phase under different error ranges for the data shown in Table 18 and Table 19. It is observed from Fig. 14 and Fig. 15 that about 98 % and 53 % proportion of fault cases are within the ±5 % error range in the estimated fault location.

A comparison of the proposed protection scheme with the existing protection schemes is presented in Table 20. Since, the proposed protection technique uses only phase current information for the protection task, it requires only current transformer. The cost of potential transformer can be saved as the voltage information is not required for the protection task. The sending end bus data is utilized, therefore there is no requirement of communication link and hence no communication latency. As smaller sampling frequency (1.2 kHz) is used the cost of digital fault recorder, computational complexity, and data storage/handling problem can be minimized. Unlike the other multi-ANN modules technique for fault detection and classification, the proposed technique uses only single ANN module that greatly reduces the computational burden and good deal of time for training and selection of the optimal architecture of multi-ANN modules.

5. Conclusion

In the present work, a protection scheme based on DWT and ANN is proposed for the complete protection of the six-phase transmission line. A single ANN_FDC module is proposed to identify and classify all the 120 types of faults. The performance of this module is evaluated w.r.t training and testing data in terms of accuracy and dependability. The performance indices show that the proposed FDC module is efficient and effective with 99.76 % accuracy. Moreover, the proposed technique is resistant to the fault parameter variations and detects all types of faults within one cycle time (16.67 ms). The ANN_FLE fault location estimation modules are proposed for approximating the fault location. The performance of all the FLE modules is also evaluated w.r.t training and testing data. The performance of the fault location estimation

Table 18. No. of 1-LG fault cases under each range of percentage error in the estimated fault location (w.r.t testing data)

		No. of fault cases					
Fault Location Module	Phase	% E1: -1% to +1%	% E2: -2% to -1% and +1% to +2%	% E3: -3% to -2% and +2% to +3%	% E4: -4% to -3% and +3% to +4%	% E5: -5% to -4% and % +4% to +5%	% E6: -10% to -5% and +5% to +10%
ANN_FLE _1-LG module (48 fault cases for each phase)	A	41	7	0	0	0	0
	B	30	4	5	5	1	3
	C	34	8	2	3	1	0
	D	38	6	2	1	1	0
	E	27	10	4	6	0	1
	F	29	14	3	2	0	0
6 × 48 = 288	1-LG	199	49	16	17	3	4

Table 19. No. of fault cases under each range of percentage error in the estimated fault location (w.r.t testing data)

		No. of fault cases					
Fault Location Module	Phase	% E1: -1% to +1%	% E2: -2% to -1% and +1% to +2%	% E3: -3% to -2% and +2% to +3%	% E4: -4% to -3% and +3% to +4%	% E5: -5% to -4% and % +4% to +5%	% E6: -10% to -5% and +5% to +10%
All fault location estimation modules. (3024 fault cases per phase)	A	439	365	258	238	189	1535
	B	470	381	275	244	190	1464
	C	589	376	291	224	202	1344
	D	456	338	283	228	195	1524
	E	493	412	313	249	199	1358
	F	463	402	281	254	216	1408
6 × 3024 = 18144	All faults	2910	2274	1701	1437	1191	8633

Table 20. Comparison of proposed scheme with other existing schemes

S. No.	Comparison term	[16]	[19]	[18]	[30]	[31]	Proposed
1.	Protection technique	ANN	Fuzzy inference system	Decision tree and TLBO tuned ANN	Adaptive PSO tuned ANN	Bat algorithm tuned deep neural network	ANN
2.	Signal pre-processing technique	DFT	DFT	Least square Adaline algorithm	DWT	Stacked encoder-grayscale images	DWT
3.	Voltage or current information requirement	Voltage and current	Voltage and current	Voltage	Voltage and current	Voltage and current	Current
4.	No. of FDC modules	11	7	11	11	11	1
5.	No. of fault cases	4930	-	28830	21600	4836	5761
6.	FDC accuracy	100 %	98.02 %	99.64 %	100 %	99.45 %	99.76 %
7.	FDC time	16.67 ms	16.67 ms	12.4 ms	14 ms	16.67 ms	16.67 ms
8.	No. of FLE modules	11	-	11	11	-	11

modules is better with training data where 81 % of the fault cases are within the ± 1 % error range but the performance w.r.t testing data is nominal where 53 % of the fault cases are within ± 5 % error range. It can be concluded that the proposed protection scheme works efficiently for fault detection and classification with a single module and the performance of fault location estimation modules can be further improved with optimal tunning of ANN parameters.

Availability of data and material

There are no new data generated in this work. Whatever data used are available openly and cited properly. Moreover, the new findings in this work kept openly.

Competing Interests

The authors declare that they have no competing interests.

Funding

Not Applicable

References

[1] I. R. E. Agency, "Renewable capacity statistics 2021,"Renew. *Renew. Capacit. Stat.*, 2021.

[2] N. B. Bhatt, S. S. Venkata, W. C. Guyker, and W. H. Booth, "Six-phase (multi-phase) power transmission systems: fault analysis," *IEEE Trans. Power Appar. Syst.*, vol. 96, no. 3, pp. 758–767, 1977.

[3] S. Venkata, W. Guyker, W. Booth, J. Kondragunta, N. Bhatt, and N. Saini, "Eppc-a computer program for six-phase transmission line design," *IEEE Trans. Power Appar. Syst.*, no. 7, pp. 1859–1869, 1982.

[4] S. Venkata, W. Guyker, W. Booth, J. Kondragunta, N. Saini, and E. Stanek, "138-kv, six-phase transmission system:

fault analysis," *IEEE Trans. Power Appar. Syst.*, no. 5, pp. 1203–1218, 1982.

[5] E. Koley, A. Yadav, and A. Thoke, "Six phase to ground fault detection and classification of transmission line using ann," *Int. J. Comput. Appl.*, vol. 41, no. 4, 2012.

[6] Q. Li, Y. Li, S. Rowland, J. Hu, I. Cotton, and X. Jiang, "Audible noise evaluation for six-phase overhead lines transformed from existing three-phase double circuit infrastructures with uprated voltages," *High Volt.*, vol. 7, no. 5, pp. 866–876, 2022.

[7] S. Shen, B. Cao, P. Crossley, Z. Wang, and X. Ding, "Transformation of a three-phase double-circuit overhead transmission line into a six-phase feeder to increase power transfer capability," *IET Gener. Transm. Distrib.*, vol. 16, no. 23, pp. 4663–4671, 2022.

[8] M. Abasi, M. Joorabian, A. Saffarian, and S. G. Seifossadat, "A comprehensive review of various fault location methods for transmission lines compensated by facts devices and series capacitors," *J. Oper. Autom. Power Eng.*, vol. 9, no. 3, pp. 213–225, 2021.

[9] H. Shad, M. Gandomkar, and J. Nikoukar, "An improved optimal protection coordination for directional overcurrent relays in meshed distribution networks with dg using a novel truth table," *J. Oper. Autom. Power Eng.*, vol. 11, no. 3, pp. 151–161, 2023.

[10] P. Venkata, V. Pandya, and A. Sant, "Data mining model based differential microgrid fault classification using svm considering voltage and current distortions," *J. Oper. Autom. Power Eng.*, vol. 11, no. 3, pp. 162–172, 2023.

[11] S. Tiwari, G. K. Singh, and A. B. Saroor, "Multiphase power transmission research—a survey," *Electr. Power Syst. Res.*, vol. 24, no. 3, pp. 207–215, 1992.

[12] G. C. Sekhar and P. Subramanyam, "Protection of six phase transmission system of allegheny power system, usa against shunt faults," in *2014 International Conference on Smart Electric Grid (ISEG)*, pp. 1–7, IEEE, 2014.

[13] E. Koley, A. Jain, A. Thoke, A. Jain, and S. Ghosh, "Detection and classification of faults on six phase transmission line using ann," in *2011 2nd International Conference on Computer and Communication Technology (ICCCT-2011)*, pp. 100–103, IEEE, 2011.

[14] R. Kumar, E. Koley, A. Yadav, and A. Thoke, "Fault classification of phase to phase fault in six phase transmission line using haar wavelet and ann," in *2014 International Conference on Signal Processing and Integrated Networks (SPIN)*, pp. 5–8, IEEE, 2014.

[15] E. Koley, A. Yadav, and A. Thoke, "Artificial neural network based protection scheme for one conductor open faults in six phase transmission line," *Int. J. Comput. Appl.*, vol. 101, no. 4, pp. 42–46, 2014.

[16] E. Koley, A. Yadav, and A. S. Thoke, "A new single-ended artificial neural network-based protection scheme for shunt faults in six-phase transmission line," *Int. Trans. Electr. Energy Syst.*, vol. 25, no. 7, pp. 1257–1280, 2015.

[17] E. Koley, K. Verma, and S. Ghosh, "A modular neuro-wavelet based non-unit protection scheme for zone identification and fault location in six-phase transmission line," *Neural Comput. Appl.*, vol. 28, pp. 1369–1385, 2017.

[18] S. K. Shukla, E. Koley, S. Ghosh, and D. K. Mohanta, "Enhancing the reliability of six-phase transmission line protection using power quality informatics with real-time validation," *Int. Trans. Electr. Energy Syst.*, vol. 29, no. 9, p. e12048, 2019.

[19] A. Yadav and V. Ashok, "A relaying scheme for detection and classification of shunt faults in six-phase transmission system based on dft-fis approach," *J. Power Technol.*, vol. 98, no. 2, p. 202, 2018.

[20] M. Verma, E. Koley, and S. Ghosh, "Application of fuzzy logic for fault detection and classification in six phase transmission line," in *2017 IEEE Int. Conf. Comput. Intell. Comput. Res. (ICCIC)*, pp. 1–5, IEEE, 2017.

[21] J. Stewart and I. Grant, "High phase order-ready for application," *IEEE Trans. Power Appar. Syst.*, no. 6, pp. 1757–1767, 1982.

[22] S. P. Valsan and K. Swarup, "Wavelet transform based digital protection for transmission lines," *Int. J. Electr. Power Energy Syst.*, vol. 31, no. 7-8, pp. 379–388, 2009.

[23] A. A. Hajjar, "A high speed noncommunication protection scheme for power transmission lines based on wavelet transform," *Electr. Power Syst. Res.*, vol. 96, pp. 194–200, 2013.

[24] A. R. Adly, S. H. A. Aleem, M. A. Algabalawy, F. Jurado, and Z. M. Ali, "A novel protection scheme for multi-terminal transmission lines based on wavelet transform," *Electr. Power Syst. Res.*, vol. 183, p. 106286, 2020.

[25] A. Valabhoju, A. Yadav, M. Pazoki, and R. A. El-Sehiemy, "Optimized ensemble of regression tree-based location of evolving faults in dual-circuit line," *Neural Comput. Appl.*, vol. 33, pp. 8795–8820, 2021.

[26] H. Mustafidah, S. Hartati, R. Wardoyo, and A. Harjoko, "Selection of most appropriate backpropagation training algorithm in data pattern recognition," *arXiv preprint arXiv:1409.4727*, 2014.

[27] D. W. Marquardt, "An algorithm for least-squares estimation of nonlinear parameters," *Journal of the society for Industrial and Applied Mathematics*, vol. 11, no. 2, pp. 431–441, 1963.

[28] M. T. Hagan and M. B. Menhaj, "Training feedforward networks with the marquardt algorithm," *IEEE trans. neural netw.*, vol. 5, no. 6, pp. 989–993, 1994.

[29] M. Akke and J. T. Thorp, "Some improvements in the three-phase differential equation algorithm for fast transmission line protection," *IEEE Trans. Power Deliv.*, vol. 13, no. 1, pp. 66–72, 1998.

[30] S. K. Shukla, E. Koley, and S. Ghosh, "A hybrid wavelet–apso–ann-based protection scheme for six-phase transmission line with real-time validation," *Neural Comput. Appl.*, vol. 31, pp. 5751–5765, 2019.

[31] T. Rao Althi, E. Koley, S. Ghosh, and S. K. Shukla, "Six phase transmission line protection using bat algorithm tuned stacked sparse autoencoder," *Electr. Power Compon. Syst.*, pp. 1–18, 2022.